J. Phys. B: At. Mol. Opt. Phys. **43** (2010) 165601 (8pp) doi:10.1088/0953-4075/43/16/165601

Double ionization of H_2 by intense attosecond laser pulses

Teck-Ghee Lee[1], **M S Pindzola and F Robicheaux**

Department of Physics, Auburn University, Auburn, AL 36849, USA

E-mail: tg10002@auburn.edu

Received 8 February 2010, in final form 21 May 2010
Published 30 July 2010
Online at stacks.iop.org/JPhysB/43/165601

Abstract

We present calculations of the double ionization of H_2 induced by an intense attosecond laser pulse at a photon energy of 40 eV using the time-dependent close-coupling method within the fixed nuclei approximation. We focus on two-photon absorption processes and examine how the response of the ejected electrons, in particular the single- and the double-energy differential probabilities, is affected by linear and circular polarizations at laser-field intensities ranging from 10^{15} W cm^{-2} to 10^{16} W cm^{-2}. In general, we find that for both linearly and circularly polarized pulses, sequential peaks and non-sequential wells that appear in both the single- and double-energy differential probabilities are akin to the analogous two-electron photoemission processes in the helium atom driven by intense attosecond pulses. In addition, for the case of a linearly polarized pulse, a clear signature of the sequential double-electron above the threshold ionization process can be seen in these spectra.

(Some figures in this article are in colour only in the electronic version)

1. Introduction

In recent years, advances in laser technology have led to the development of intense, ultrashort x-ray laser pulses with durations on the order of a few hundred attoseconds (as). Due to the timescale of an attosecond pulse being of the same order as that of electrons in atoms and molecules, there is intense interest among the atomic, molecular and optical physics communities in exploring the interaction of an intense attosecond pulse with atoms and molecules. Experimentally, ultrashort x-ray pulses with durations on the order of a few hundred attoseconds have been produced by means of the high-order harmonic generation technique [1] and may achieve intensities greater than 10^{14} W cm^{-2}. At the present time, experimental capabilities cannot realize both high intensity and short pulse duration at the same time. The present records for the shortest pulses have been reported by Sansone *et al* for a pulse length of 130 as [2] and Goulielmakis *et al* [3] for a pulse length of 80 as. It is reasonable to expect that attosecond pulses with even higher peak intensities and shorter pulse durations will be available in the near future.

The interaction of an ultrashort (e.g. femtoseconds to sub-femtoseconds) laser pulse with atoms has been the subject of recent study, particularly for two-electron systems. The experimental realization of a 950 as XUV laser pulse with a photon energy of 27.9 eV using an autocorrelation technique [4], as well as the observation of the two-photon double ionization and above threshold ionization of atomic helium induced by the Ti sapphire 27th harmonic pulse with photon energy of 41.8 eV [5], has provided a promising start.

Theoretically, substantial work has been developed for these two-electron processes. A range of methods based on the solution of the time-dependent Schrödinger equation have been applied to study the two-electron ejection process. These include the direct numerical integration of the time-dependent Schrödinger equation with a finite-difference-basis set scheme on a lattice [6], the two-electron time-dependent close-coupling method [7–9], a mixed atomic *B*-spline spectral and configuration interaction method [10, 11], the Jacobi matrix with spectral approach [12, 13] and a time-dependent Schrödinger equation method with correlated multichannel states [14, 15]. The time-independent *R*-matrix Floquet theory has also been successfully applied to study the two-photon double-ionization process of He [16]. In addition, the development of time-dependent R-matrix approaches [17, 18] allows the study of the interaction of an attosecond pulse with complex atoms. A major focus of these studies has

[1] Author to whom any correspondence should be addressed.

been to elucidate the role of the sequential and nonsequential ionization mechanisms in the two-photon double-ionization process. Intense attosecond pulses interacting with helium have been examined by Ishikawa and Midorikawa [19], Barna *et al* [20] and Lee *et al* [21].

The corresponding two-centre problem for the simplest two-electron molecule, H_2, in which the potential is now no longer spherically symmetric has not received the same attention. Two-photon double ionization of the hydrogen molecule at a photon energy of 30 eV has been studied using the time-dependent close-coupling [22] and the exterior complex scaling [23] methods. Here we study an intense attosecond pulse interacting with H_2. For an attosecond pulse the definition of a cross section is no longer meaningful as the intensity of the pulse is not so well defined as the synchrotron studies. To investigate the physics of the two-electron ejection induced by two-photon absorption, we calculate single- and double-energy differential probabilities for both linear and circular polarization.

This paper is organized as follows. In section 2, we develop the time-dependent close-coupling method as applied to the double ionization of the H_2 molecule by an intense attosecond laser pulse. In section 3, at a photon energy of 40 eV, we present single- and double-energy differential probabilities and the corresponding reduced wavefunction probability densities. In section 4, we end with a brief summary. Atomic units ($m_e = \hbar = e = 1$) are used throughout the paper unless otherwise stated.

2. Theoretical method

The time-dependent close-coupling theory presented here is a generalization of our previous work for two-electron atomic systems [7]. The time-dependent Schrödinger equation for a two-electron homonuclear diatomic molecule in a time-varying electromagnetic field is given by

$$\mathrm{i}\frac{\partial\psi(\vec{r}_1,\vec{r}_2,t)}{\partial t} = (H_{\rm mol} + H_{\rm rad})\psi(\vec{r}_1,\vec{r}_2,t). \tag{1}$$

The non-relativistic Hamiltonian for the molecule is given by

$$H_{\rm mol} = \sum_{i=1}^{2}\left(-\frac{1}{2}\nabla_i^2 - \sum_{\pm}\frac{Z}{\sqrt{r_i^2 + \frac{1}{4}R^2 \pm r_i R\cos\theta_i}}\right) + \frac{1}{|\vec{r}_1 - \vec{r}_2|}, \tag{2}$$

where $Z = 1$ for H_2, the internuclear axis is along the z axis and R is the internuclear distance. The radiation field Hamiltonian, for linear polarization with respect to the internuclear axis, is given by

$$H_{\rm rad} = E(t)\cos\omega t\sum_{j=1}^{2} z_j, \tag{3}$$

where ω is the radiation field frequency. The radiation field Hamiltonian, for circular polarization with respect to the internuclear axis, is given by

$$H_{\rm rad} = \frac{E(t)}{2\sqrt{2}}\left(\mathrm{e}^{\mp\mathrm{i}\omega t}\sum_{j=1}^{2}(x_j + \mathrm{i}y_j) + \mathrm{e}^{\pm\mathrm{i}\omega t}\sum_{j=1}^{2}(x_j - \mathrm{i}y_j)\right), \tag{4}$$

where the $(-,+)$ sign in the first exponent of the first term denotes right-circular and left-circular polarization, respectively, and note that the second term is complex conjugate to the first term. For all polarizations, the pulsed electromagnetic field is given by

$$E(t) = E_0\,\mathrm{e}^{-2\ln 2(t-2T)^2/T^2}, \tag{5}$$

where E_0 is the electric field strength and T is the full width at half maximum pulse length.

The total wavefunction is expanded in products of rotational functions for each MS symmetry:

$$\psi(\vec{r}_1,\vec{r}_2,t) = \sum_{m_1,m_2}\frac{P^{MS}_{m_1m_2}(r_1,\theta_1,r_2,\theta_2,t)}{r_1r_2\sqrt{\sin\theta_1}\sqrt{\sin\theta_2}}\Phi_{m_1}(\phi_1)\Phi_{m_2}(\phi_2), \tag{6}$$

where $\Phi_m(\phi) = \frac{\mathrm{e}^{\mathrm{i}m\phi}}{2\pi}$ and $M = m_1 + m_2$. Upon substitution of the total wavefunction of equation (6) into the time-dependent Schrödinger equation, we obtain a set of time-dependent close-coupled (TDCC) partial differential equations given by

$$\begin{aligned}\mathrm{i}&\frac{\partial P^{MS}_{m_1m_2}(r_1,\theta_1,r_2,\theta_2,t)}{\partial t}\\ &= T_{m_1m_2}(r_1,\theta_1,r_2,\theta_2)P^{MS}_{m_1m_2}(r_1,\theta_1,r_2,\theta_2,t)\\ &\quad + \sum_{m_1',m_2'}V^{M}_{m_1m_2,m_1'm_2'}(r_1,\theta_1,r_2,\theta_2)P^{MS}_{m_1'm_2'}(r_1,\theta_1,r_2,\theta_2,t)\\ &\quad + \sum_{M''}\sum_{m_1'',m_2''}W^{MM''}_{m_1m_2,m_1''m_2''}(r_1,\theta_1,r_2,\theta_2,t)\\ &\quad \times P^{M''S}_{m_1''m_2''}(r_1,\theta_1,r_2,\theta_2,t),\end{aligned} \tag{7}$$

where $P^{MS}_{m_1m_2}(r_1,\theta_1,r_2,\theta_2,t)$ is a two-electron reduced wavefunction, $T_{m_1m_2}(r_1,\theta_1,r_2,\theta_2)$ is a sum over one-electron operators, $V^{M}_{m_1m_2,m_1'm_2'}(r_1,\theta_1,r_2,\theta_2)$ is a two-electron coupling operator and $W^{MM''}_{m_1m_2,m_1''m_2''}(r_1,\theta_1,r_2,\theta_2,t)$ is a sum over one-electron radiation field coupling operators.

The initial condition for the solution of the TDCC equations is given by

$$\begin{aligned}&P^{MS}_{m_1m_2}(r_1,\theta_1,r_2,\theta_2,t=0)\\ &\quad = \bar{P}_{m\bar{m}}(r_1,\theta_1,r_2,\theta_2,\tau\to\infty)\delta_{M,0}\delta_{S,0}\delta_{m_1,m}\delta_{m_2,\bar{m}},\end{aligned} \tag{8}$$

where the two-electron reduced wavefunctions $\bar{P}_{m\bar{m}}(r_1,\theta_1,r_2,\theta_2,\tau)$ are obtained by the solution of a set of TDCC partial differential equations for the imaginary time (τ) relaxation of equation (1) with $H_{\rm rad} = 0$ and for $m + \bar{m} = M = S = 0$.

Following time propagation of the TDCC equations with an implicit algorithm (see expression (19) in [24]), the total double-photoionization probability for a particular MS symmetry is given by

$$\mathcal{P} = \sum_{l_1,m_1}\sum_{l_2,m_2}\int_0^\infty \mathrm{d}k_1\int_0^\infty \mathrm{d}k_2|P^{MS}_{l_1m_1l_2m_2}(k_1,k_2)|^2, \tag{9}$$

where

$$\begin{aligned}P^{MS}_{l_1m_2l_2m_2}(k_1,k_2) &= \int_0^\infty \mathrm{d}r_1\int_0^\pi \mathrm{d}\theta_1\int_0^\infty \mathrm{d}r_2\\ &\quad\times\int_0^\pi \mathrm{d}\theta_2 P^*_{k_1l_1m_1}(r_1,\theta_1)P^*_{k_2l_2m_2}(r_2,\theta_2)\\ &\quad\times\left(P^{MS}_{m_1m_2}(r_1,\theta_1,r_2,\theta_2,t\to\infty)\right.\\ &\quad\left.-\mathcal{L}P^{MS}_{m_1m_2}(r_1,\theta_1,r_2,\theta_2,t=0)\right);\end{aligned} \tag{10}$$

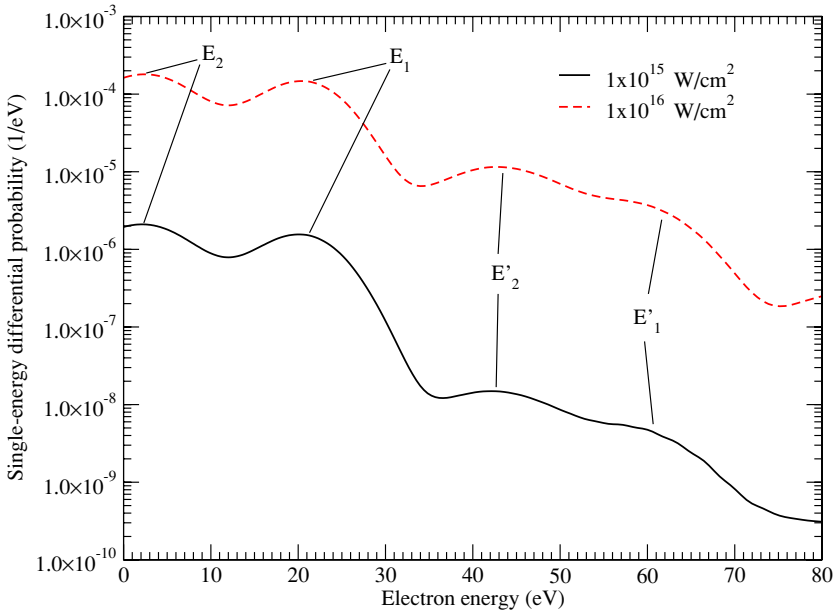

Figure 1. Single-energy differential probability $\frac{d\mathcal{P}}{dE}$ as a function of one ejected electron energy for a pulse with a total duration of $20\pi/\omega$.

the overlap function is given by

$$\mathcal{L} = \int_0^\infty dr_1 \int_0^\pi d\theta_1 \int_0^\infty dr_2 \int_0^\pi d\theta_2 \, P^{MS}_{m_1 m_2}(r_1, \theta_1, r_2, \theta_2, t = 0) \times P^{MS}_{m_1 m_2}(r_1, \theta_2, r_2, \theta_2, t \to \infty) \quad (11)$$

and $P_{klm}(r, \theta)$ are the H_2^+ continuum distorted wavefunctions. A single-energy differential double-photoionization probability is given by

$$\frac{d\mathcal{P}}{dE_1} = \sum_{l_1, m_1} \sum_{l_2, m_2} \frac{1}{k_1} \int_0^\infty dk_2 \left| P^{MS}_{l_1 m_1 l_2 m_2}(k_1, k_2) \right|^2, \quad (12)$$

while a double-energy differential double-photoionization probability is given by

$$\frac{d^2\mathcal{P}}{dE_1 \, dE_2} = \sum_{l_1, m_1} \sum_{l_2, m_2} \frac{1}{k_1 k_2} \left| P^{MS}_{l_1 m_1 l_2 m_2}(k_1, k_2) \right|^2. \quad (13)$$

In addition, a reduced wavefunction probability density is given by

$$\phi^{MS}_{m_1 m_2}(r_1, r_2) = \left| \int_0^\pi d\theta_1 \int_0^\pi d\theta_2 \, P^{MS}_{m_1 m_2}(r_1, \theta_1, r_2, \theta_2, t \to \infty) \right|^2. \quad (14)$$

3. Results and discussion

In this work, we focus on two electrons instantaneously ejected from the ground state of H_2 (at the equilibrium internuclear separation of $R_e = 1.4$ au) when the molecule is subjected to a 10 optical-cycle laser pulse whose photon energy is 40 eV ($\hbar\omega = 1.47$ au) and whose total pulse duration is $20\pi/\omega$ au. We consider in our calculations both the cases where the pulse is linearly and circularly polarized at field intensities ranging from 10^{15} W cm^{-2} to 10^{16} W cm^{-2}.

The time-dependent Schrödinger equation is solved using the close-coupling method on a numerical lattice. Before performing the dynamics calculations, the Schrödinger equation is relaxed on the lattice with 250 imaginary time steps, using $\Delta\tau = 0.02$ au with three terms in the expansion over rotation wavefunctions for the $M = 0$ symmetry in order to yield a correlated ground-state eigenfunction of H_2 with an eigenenergy of -52.7 eV compared to the exact value of the ground-state ionization energy of -51.5 eV. The close-coupled equations with the radiation field are then solved on a uniform mesh using a standard finite difference scheme. We utilize a lattice size of $384 \times 384 \times 16 \times 16$ points with a radial mesh spacing of $\Delta r_1 = \Delta r_2 = 0.2$ au such that we reach a maximum box size of 76.8 au and an angular mesh spacing of $\Delta\theta_1 = \Delta\theta_2 = 0.0625\pi$ that subtends from 0 to π radians. The TDCC equations are propagated for ten radiation field periods. In the case of a linearly polarized pulse, three coupled channels are employed for the $M = 0$ symmetry. For a circularly polarized case, 14 coupled channels are employed for the $M = 0$–3 symmetries. The rotational-channel combinations included in the close-coupling calculations are $-1 \leqslant \{m_1, m_2\} \leqslant 3$. It is noteworthy to mention that the present calculations are computationally intensive with each run using up to 10^4 processors for an average of 12 hours on a CRAY XT5 supercomputer.

3.1. Linearly polarized pulse

The total double-ionization probability from equation (9) for a linearly polarized pulse at 10^{15} W cm^{-2} is found to be 3.65×10^{-5}, rising to 3.56×10^{-3} at 10^{16} W cm^{-2}, that is a jump of two orders of magnitude. The single-energy differential probability $\frac{d\mathcal{P}}{dE}$ from equation (12) is presented in figure 1 for the two different intensities. Except for the two orders of magnitude difference, the behaviour and features of these two curves are essentially identical. Note that each curve exhibits two notable peaks followed by a formation of two

smaller peaks. Namely, the first set constitutes $E_1 \sim 21$ eV and $E_2 \sim 3$ eV and the second set consists of $E_1' \sim 43$ eV and $E_2' \sim 61$ eV. E_1 and E_2 are located quite close to the energies of $\epsilon_1 = \hbar\omega - I^+$ and $\epsilon_2 = \hbar\omega - I^{2+}$, where $I^+ = 15.4$ eV and $I^{2+} = 36.1$ eV are the ionization potential energies of H_2 and H_2^+, respectively. The E_1 and E_2 peaks are due to two photons predominantly being absorbed one after another in a sequential manner. In other words, the first photon being absorbed by H_2 ionizes one of the electrons in its ground state and the subsequent photon ionizes the remaining electron in the ground state of H_2^+. This feature is similar to what Lee *et al* [21] and others [19, 20, 25] have encountered previously in the case of the two-photon double ionization of He by intense attosecond pulse where the laser pulse length is compatible to the one presented here. Thus, this finding is an 'acid test' and gives us confidence in our calculations in the absence of other theory or experiment for us to compare with at this moment.

The secondary pair of peaks, E_1' and E_2', is rather interesting as their energy positions approximately correspond to the absorption of two photons by each electron at $\epsilon_1' = 2\hbar\omega - I^+$ and $\epsilon_2' = 2\hbar\omega - I^{2+}$. This feature, within the presented intensity range, could only come from the so-called sequential double-electron above-threshold ionization (S-DATI) process, which was again first predicted in the intense field double ionization of atomic He, induced by a rather long 46-field period laser pulse with photon energy of $\hbar\omega = 87$ eV and at a peak intensity of 2×10^{16} W cm^{-2} [6].

The energy difference between $E_1(E_1')$ and $E_2(E_2')$ is around 18 eV. The origin of this difference can be easily explained from the difference between the first and second ionization potential of the molecule (i.e. ~20.7 eV). Note that the slight shift (~2%) in energy for $E_1(E_1')$ and $E_2(E_2')$ from $\epsilon_1(\epsilon_1')$ and $\epsilon_2(\epsilon_1')$ may be attributed to the grid spacing we used in our calculations.

We next compare the contour landscape for the double-energy differential probability $\frac{d^2\mathcal{P}}{dE_1 dE_2}$ of equation (13) as functions of photoelectron energies for the two laser intensities in figure 2. These contours have a broad energy width along the equal energy sharing direction and the spectra closely resemble the He case when the pulse length is very short and of the order of ~100 as (e.g. see figure 3(c) in [21]). The S-DATI electron distribution discussed earlier in the single-energy spectra is also clearly reflected on the contour plot for a laser peak intensity of 10^{16} W cm^{-2}.

In figure 3, we show the reduced wavefunction probability densities $\phi^{MS}_{m_1 m_2}(r_1, r_2)$ of equation (14) for the $\{0, 0\}$ and $\{1, -1\}$ channels after the continuum wavefunctions have been propagated to the final time $t_f = 43$ au. Again, a comparison is made between the two laser intensities. For calculations with such a high laser intensity, we were concerned about the adequacy of our box size as the fast electron density can reflect from the boundary of the box. Now, judging from the spread of the density shown in figure 3, we are certain that the box size we used is ample for the present calculations. Figure 3 indicates that most of the ionization flux is coming from the $\{0, 0\}$ channel. It also shows that the high density of the flux is generally concentrated in a small

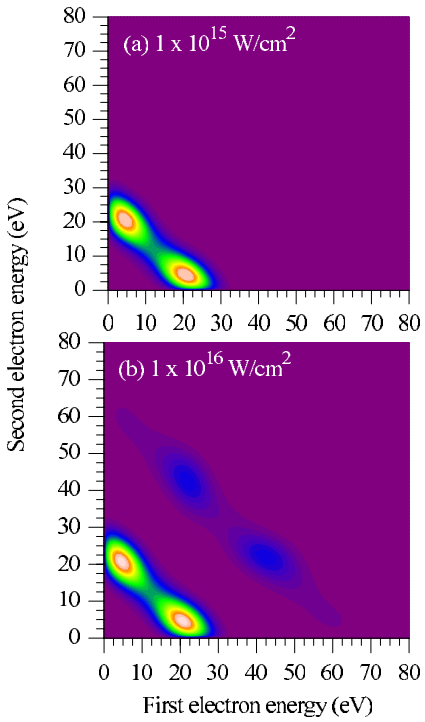

Figure 2. Contour plots of the double-energy differential probability $\frac{d^2\mathcal{P}}{dE_1 dE_2}$ (in arbitrary unit) as a function of both ejected electron energies at intensities of (a) 10^{15} W cm^{-2} and (b) 10^{16} W cm^{-2}. The second snapshot shows a clear signature of S-DATI for a pulse with 10^{16} W cm^{-2}. Note that the 'conjoint-lobe' enclosed by the lighter shading represents the maxima of the probability density.

radial distance, i.e. r_1 and $r_2 < 10$ au, while we note that single ionization resides along the r_1 and r_2 axes. The most intriguing result is the one illustrated in figure 3(b1), in which the probability density associated with double ionization is rather spread out, but concentrates mostly in the middle of the plot. Comparing this with a recent investigation of dynamical screening in two-photon double ionization of He (cf figure 1 in [26]), even though our applied laser pulse in this case is much shorter and intense than theirs, we find a general similarity in the behaviour of the density distribution. This leads us to conclude that the 'middle-gathering' in our probability density plot may suggest some kind of dynamical screening. Also, note that there are some small oscillations on the contour map. We have checked the results by including extra coupled channels in our close-coupling calculations. The results we obtained with five coupled channels are practically identical. The oscillations in the reduced wavefunctions are real and may be attributed to the interference between the outgoing single-electron continuum wavepacket and the correlated two-electron continuum wavepacket. It is worthwhile to note that our total double-ionization probability at a laser intensity of 10^{16} W cm^{-2} for three coupled channels and five coupled channels is calculated to be 3.560×10^{-3} and 3.562×10^{-3}, respectively. Increasing the coupled channels retained in our close-coupling expansion made a negligible difference for the

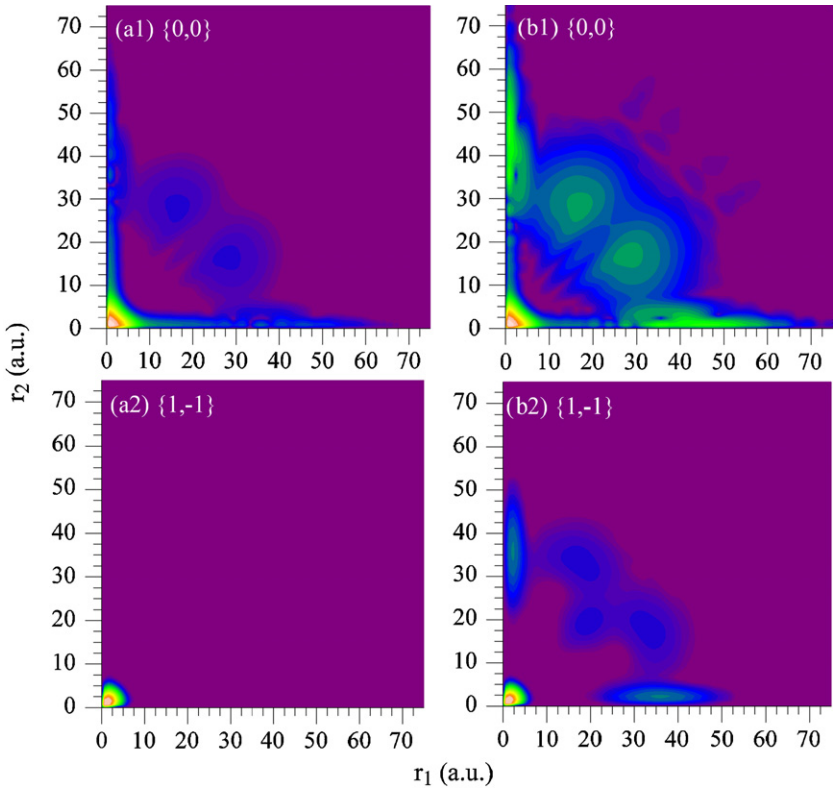

Figure 3. Contour plots of reduced wavefunction probability densities (in arbitrary unit) at the end of the pulse duration for the {0, 0} and {1, −1} coupled channels. Note that (a1) and (a2) are for an intensity of 10^{15} W cm^{-2}, and (b1) and (b2) are for 10^{16} W cm^{-2}.

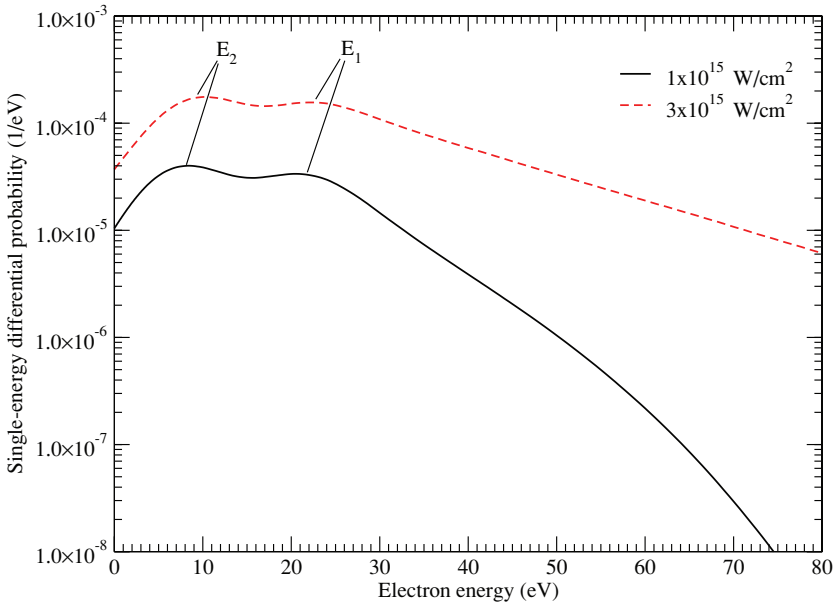

Figure 4. Same as figure 1, but from a 14 coupled channel calculation for a circularly polarized pulse.

calculations presented here, illustrating the convergence of our calculations.

3.2. Circularly polarized pulse

Now we shall turn to explore what will happen to the single- and double-energy differential probabilities, as well as their corresponding reduced wavefunction probability densities, for double ionization of the hydrogen molecule if circularly polarized light is used. First, note that our total double-ionization probability for a circularly polarized pulse at a laser intensity of 10^{15} W cm^{-2} is found to be 1.12×10^{-3}. This is about 30 times larger than the linearly polarized case and is somewhat larger than the case of one-photon double

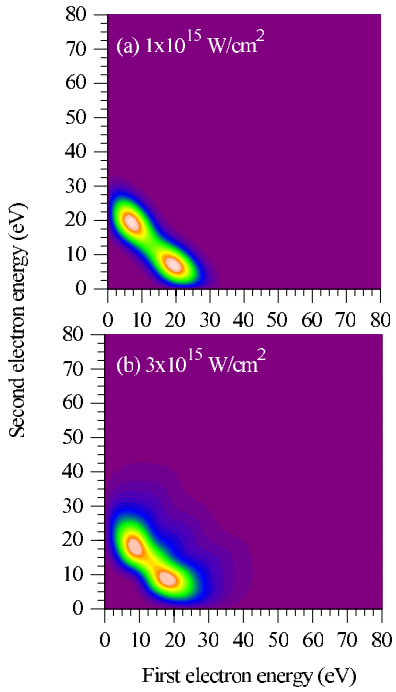

Figure 5. Same as figure 2, but from a 14 coupled channel calculation for a circularly polarized pulse.

ionization of H_2 [27]. There, at roughly the same intensity, the one-photon double-ionization cross section for a circularly polarized radiation is found to be only ∼10 times greater than the linear one. At this stage, it is essential to note that we have carried out the calculation for an intensity of 10^{16} W cm^{-2}, but our double-ionization results are contaminated with the reflection from the boundaries. As a result, we scaled down to an intensity of 3×10^{15} W cm^{-2}. The total double-ionization probability for the 3×10^{15} W cm^{-2} is found to be 9.07×10^{-3}. This is roughly a factor of 10 increase in the ionization probability with intensity increased by a factor of 3.

In figure 4, we present the single-energy differential probability $\frac{d\mathcal{P}}{dE}$ as a function of photoelectron energy at intensities of 10^{15} and 3×10^{15} W cm^{-2}. Below the photoelectron energy of 30 eV, there exist two sequential peaks similar to the one that we observed previously in the linearly polarized case. But here we do not see the second-order peaks due to the S-DATI processes. The shape of the curves, especially in the region of high photoelectron energy, are not quite the same as we have seen in figure 1. To make sure that the presented results are reasonably stable for an intensity of 3×10^{15} W cm^{-2}, we made further checks on our 14-channel (i.e. channels that coupled to the $M = 0$–3 symmetries) results by performing larger calculations with 16 coupled channels that include two more $M = 2$ symmetries. We find that the difference in the total two-photon double ionization and the single-energy differential probabilities obtained between 14- and 16-channel calculations is less than 1%. However, as we further increased the number of coupled channels from 14 to 17 that include three $M = 4$ symmetries, and to 18 that include four $M = -1$ symmetries, we find our total double-ionization probabilities to be 9.30×10^{-3} and 9.38×10^{-3},

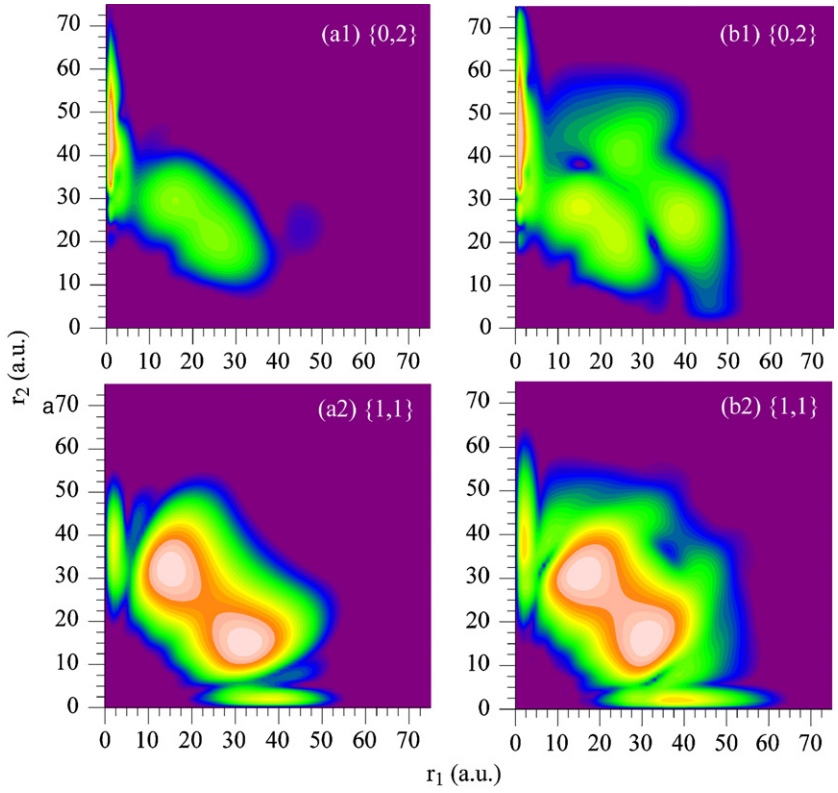

Figure 6. Same as figure 3, but from a 14 coupled channel calculation for a circularly polarized pulse. The dominant coupled channels are {0, 2} and {1, 1}, and (a1) and (a2) are for 10^{15} W cm^{-2}, while (b1) and (b2) are for 3×10^{15} W cm^{-2}.

respectively. Comparing these values to 9.03×10^{-3} from the 14-channel calculation, we have a 3% change. Furthermore, although not shown here, we also noted that there is a slight change in the relative heights of the two sequential peaks in the single-energy differential probabilities in both the 17- and 18-channel calculations.

We now examine the contour landscapes of their corresponding double-energy differential probability $\frac{d^2\mathcal{P}}{dE_1 dE_2}$ as functions of photoelectron energies in figure 5. These landscapes reveal that the energy spectra for both intensities are generally similar to the linearly polarized one. The S-DATI electron distribution is obviously absent. At 3×10^{15} W cm^{-2}, we also see some broadening and stretching of the spectrum along the equal energy sharing direction. It seems, at high intensity, the circularly polarized pulse has altered the photoemission energy spectra of the two electrons. The feature is genuine as we confirmed it with the larger coupled channel calculations.

Finally, we show the reduced wavefunction probability densities $\phi^{MS}_{m_1 m_2}(r_1, r_2)$ for $\{0, 2\}$ and $\{1, 1\}$ channels in figure 6. Note that we do not show the density for the $\{2, 0\}$ channel because it is essentially a mirror image of the $\{0, 2\}$ with reflection along the $r_1 = r_2$ axis. It is clear that the $\{1, 1\}$ symmetric channel is the dominant one for both intensities. There is a noticeable single-ionization component in the $\{0, 2\}$ (and $\{2, 0\}$) channel that appears along the r_2 (and r_1) axis. However, it is the $\{1, 1\}$ channel that has most of the density and is mainly concentrated in the large radial region, i.e. between $\sim$20 and $\sim$50 au. This characteristic is somewhat similar to, but more intense than, the linearly polarized case seen earlier, which may signal that the S-DATI process is inherently there but cannot be effectively revealed with a circularly polarized pulse. Once more, by comparing to the linearly polarized case, we observe more severe and widely spread oscillations on the contour landscapes and again the notion may be attributed to interference between the outgoing single-electron and the outgoing two-electron continuum wavepackets.

4. Conclusions

In this study, we have investigated the double-electron photoemission process from a hydrogen molecule driven by an intense attosecond laser pulse with a photon energy of 40 eV by solving the two-electron time-dependent close-coupling equations within the fixed nuclei approximation for different laser intensities and polarizations. In particular, we concentrated on two-photon absorption processes and analysed the two-electron ejected single- and double-energy differential probabilities, as well as their corresponding reduced wavefunction probability densities. In the absence of other theoretical or experimental work for the hydrogen molecule, we contrasted our results to the 'more familiar' case of helium atoms in intense laser fields.

We found that there exist sequential peaks and non-sequential wells in both the single- and double-energy differential probabilities for the linearly and circularly polarized pulses at laser-field intensities ranging from 10^{15} W cm^{-2} to 10^{16} W cm^{-2}. Generally, these features are akin to the analogous two-electron photoemission processes in the helium atom. In the linearly polarized case, in addition to the traditional peaks due to sequential processes, we also observed a secondary pair of peaks that arise from the sequential double-electron above threshold ionization process. In the analysis, we also found that the so-called sequential double-electron above threshold ionization process could only be clearly revealed when a linearly polarized pulse is used. In addition, we see some oscillations in the contour maps of the reduced wavefunction probability density that may be due to the interference between the outgoing one-electron and two-electron continuum wavepackets. Furthermore, convergence studies were also carried out with respect to the number of coupled channels included in our close-coupling calculations in order to ensure that our calculations are reasonably accurate for the intensities we examined. Finally, with the rapid progress in the technological development of ultrashort and high power laser pulses, we hope this work will serve as a motivation for future experimental studies.

Acknowledgments

This work was supported in part by grants from the US National Science Foundation and the Department of Energy. Computational work was carried out at the National Energy Research Scientific Computing Center in Oakland, California and at the National Institute for Computational Sciences in Knoxville, Tennessee.

References

[1] Kienberger R *et al* 2004 *Nature* **427** 817
[2] Sansone G *et al* 2006 *Science* **314** 443
[3] Goulielmakis E *et al* 2008 *Science* **320** 1614
[4] Sekikawa T *et al* 2004 *Nature* **432** 605
[5] Hasegawa H *et al* 2005 *Phys. Rev.* A **71** 023407
[6] Parker J S *et al* 2001 *J. Phys. B: At. Mol. Opt. Phys.* **34** L69
[7] Pindzola M S and Robicheaux F 1998 *J. Phys. B: At. Mol. Opt. Phys.* **31** L823
[8] Colgan J and Pindzola M S 2002 *Phys. Rev. Lett.* **88** 173002
[9] Pindzola M S *et al* 2007 *J. Phys. B: At. Mol. Opt. Phys.* **40** R39
[10] Laulan S and Bachau H 2003 *Phys. Rev.* A **68** 013409
[11] Laulan S and Bachau H 2004 *Phys. Rev.* A **69** 033408
[12] Foumouo E *et al* 2006 *Phys. Rev.* A **74** 063409
[13] Foumouo E *et al* 2008 *J. Phys. B: At. Mol. Opt. Phys.* **41** 051001
[14] Nikolopoulos L A A and Lambropoulos P 2007 *J. Phys. B: At. Mol. Opt. Phys.* **40** 1347
[15] Lambropoulos P and Nikolopoulos L A A 2008 *New J. Phys.* **10** 025012
[16] Feng L and van der Hart H W 2003 *J. Phys. B: At. Mol. Opt. Phys.* **36** L1
[17] Lysaght M A, van der Hart H W and Burke P G 2009 *Phys. Rev.* A **79** 053411
[18] Xiaoxu Guan *et al* 2009 *J. Phys.: Conf. Ser.* **194** 032027
[19] Ishikawa K L and Midorikawa K 2005 *Phys. Rev.* A **72** 013407

[20] Barna I F, Wang J and Burgdörfer J 2006 *Phys. Rev.* A **73** 023402
[21] Lee T-G, Pindzola M S and Robicheaux F 2009 *Phys. Rev.* A **79** 053420
[22] Colgan J, Pindzola M S and Robicheaux F 2008 *J. Phys. B: At. Mol. Opt. Phys.* **41** 121002
[23] Morales F *et al* 2009 *J. Phys. B: At. Mol. Opt. Phys.* **42** 134013
[24] Pindzola M S, Ludlow J A and Colgan J 2009 *Phys. Rev.* A **80** 032707
[25] Foumouo E *et al* 2008 *New J. Phys.* **10** 025017
[26] Foumouo E *et al* 2010 *J. Phys. B: At. Mol. Opt. Phys.* **43** 091001
[27] Colgan J, Pindzola M S and Robicheaux F 2004 *J. Phys. B: At. Mol. Opt. Phys.* **37** L337